Light-Triggered Reversible Tuning of Second-Harmonic Generation in a Photoactive Plasmonic Molecular Nanocavity

Danjun Liu[a,b,#] *Yunxia Wang*[a,#] *Qiang Zhang*[c,#] *Ye Ming Qing*[a], *Yaorong Wang*[a], *Haitao Huang*[b], *Chi Wah Leung*[b], *and Dangyuan Lei*[a,*]

[a] Department of Materials Science and Engineering, City University of Hong Kong, 83 Tat Chee Avenue, Kowloon, Hong Kong S.A.R.

[b] Department of Applied Physics, The Hong Kong Polytechnic University, 11 Yuk Choi Road, Hung Hom, Hong Kong S.A.R.

[c] College of Optoelectronics, and Key Lab of Advanced Transducers and Intelligent Control System of Ministry of Education, Taiyuan University of Technology, Taiyuan 030024, China

* Email: dangylei@cityu.edu.hk

ABSTRACT: The ultrasmall mode volume and ultralarge local field enhancement of compact plasmonic nanocavities have been widely explored to amplify a variety of optical phenomena at the nanoscale. Other than passively generating near-field enhancements, dynamic tuning of their intensity and associated nonlinear optical processes such as second-harmonic generation (SHG) plays a vital role in the field of active nanophotonics. Here we apply host-guest molecular complex to construct a photoswitchable molecule-sandwiched metallic particle-on-film nanocavity (MPoFN) and demonstrate both light-controlled linear and nonlinear optical tuning. Under

alternating illumination of ultraviolet (UV) and visible lights, the photoactive plasmonic molecular nanocavity shows reversible switching of both surface-enhanced Raman scattering (SERS) and plasmon resonance. Surprisingly, we observe more significant modulation of SHG from this photoactive MPoFN, which can be explained qualitatively by the quantum conductivity theory (QCT). Our study could pave the way for developing miniaturized integrated optical circuits for ultrafast all-optical information processing and communication.

KEYWORDS: host-guest molecular complex, metallic particle-on-film nanocavity, second-harmonic generation, quantum conductivity theory

The last two decades have witnessed a rapid growth of the use of plasmonic nanostructures to enhance optical signals, with the hope of significantly improving the efficiency and shrinking the size of traditional optoelectronic devices, which led to the birth of many plasmon-enhanced optical spectroscopies.[1-4] Recently, plasmonic nanostructures have been utilized to enhance the nonlinear optical response of noble metals, including second- and third-harmonic generation (S/THG),[5-9] four-wave mixing (FWM)[10] and two-photon photoluminescence (TPPL).[11-14] It is worth noting that although the centrosymmetric lattice arrangement of bulk gold and silver forbids the occurrence of SHG within the electric-dipole approximation, the surface effects of a plasmonic nanostructure (for example sphere nanoparticles[15] or flat metal film[16]) would break the inversion symmetry of bulk materials and produce observable SH nonlinear signals. This is achieved through simultaneously enhancing the symmetry-breaking-induced local surface contribution and also invoking the nonlocal bulk contribution from the magnetic dipoles and electric quadrupoles in the near-surface region of the nanostructure.

Among all the metal nanostructures that have been studied in the context of nonlinear plasmonics, of particular interest is the plasmonic nanocavity consisting of a metal nanoparticle separated from metal film by a nanometer-thick self-assembled monolayer (SAM) of molecules or a dielectric oxide layer (so-called plasmonic metal particle-on-film nanocavities (MPoFNs)). This system provides a versatile platform for nonlinear plasmonics.[17-21] For instance, efficient SHG and THG have been demonstrated in this system and used to achieve ultrasensitive nonlinear nanorulers[17] and probe the quantum tunneling limit of plasmonic near-field enhancement.[19] In addition to the popularity in nonlinear plasmonics, this fascinating system has also been applied to study plasmon resonance tuning and mode hybridization,[22-25] enhanced Raman scattering,[2, 26, 27] quantum plasmonics,[19, 28-31] single-molecule strong coupling[32, 33] and so forth. However, all these demonstrations were made in a passive manner. Specifically, the nonlinear optical signals were modulated passively through simply adjusting the particle-film gap distance. Although active control of the optical emissions in the MPoFN has been widely demonstrated by using the electrochemical potential[34, 35] as well as thermoresponsive materials.[36, 37] Up to now, active control of the nonlinear optical phenomena in such nanocavities using external stimuli such as electric and magnetic fields, has been seldom investigated. In fact, realization of active modulation of nonlinear plasmonics in a reversible manner and at ultrafast timescales is of great importance for a variety of active nanophotonics applications, particularly for information processing[38] and designing highly integrated nanophotonics devices.[39]

In this study, we demonstrate all-optical control of both linear and nonlinear emissions in a photoactive molecule-sandwiched MPoFN by using light-controlled molecular conductance switching. Here, individual gold nanospheres (Au NSs) are firstly functionalized with a nanometer-thick SAM of a host-guest molecular system (namely the photochromic diarylethene

(DAE) as guest and thiol-β-cyclodextrin (CD) as host), and then the molecular complex-capped Au NSs are drop-casted onto a gold thin film to form isolated plasmonic molecular nanocavities. At the single-particle level, we observe light-controlled switching of surface-enhanced Raman scattering (SERS) signals from the photoactive DAE molecule under alternating ultraviolet (UV)-visible light illumination, which is correlated with the reversible tuning of the cavity's vertically bonding dipolar plasmon resonance mode (more sensitive to the cavity's dielectric environment). Specifically, switching the cavity's molecular junction to the "on" state under UV light illumination induces a reduction of peak intensity in the vertically coupled plasmon resonance mode; subsequent visible-light illumination restores the junction to its "off" state and hence increases the peak intensity to its initial level. More important, we observe even more significant reversible modulation of SHG from the photoactive MPoFN through light-triggered molecular conductance switching, potentially enabling tremendous flexibilities in manipulating the nonlinear response and ultrafast dynamics of plasmonic molecular nanocavities interfaced with molecular electronics.

Active tuning of optical phenomena in plasmonic nanostructures using photochromic compounds has become a hot topic under investigation.[40, 41] It is well known that photochromic molecules can be classified into two categories, thermally reversible and irreversible compounds.[42] Azobenzene and spirobenzopyran belong to the former; furylfulgide and dithienylethene (thermally irreversible but photochromic) to the latter. Among the thermally irreversible compounds, diarylethene (DAE) with heterocyclic aryl groups is a promising candidate for practical applications because of its exceptional thermal stability and fatigue-resistant characteristics.[43-45] The photochromic reaction process of DAE is based on the reversible hexatriene-cyclohexadiene type photocyclization. Unfortunately, the open ring form of DAE has two different conformations, parallel and

antiparallel. The photocyclization can only proceed from the antiparallel conformation while the parallel conformation is photochemically inactive.[46, 47] To assist the antiparallel conformation, DAE is usually embedded into the bowl-like cyclodextrin (CD) cavities and therefore the photocyclization quantum yield of DAE is increased.[46]

Based on above-mentioned rational, we use DAE (guest) and thiol-β-CD (host) to form active plasmonic molecular nanocavities. Figure 1a shows the absorption spectra of the host-guest molecular complex in dimethylformamide (DMF) solution before and after UV or visible light illumination. Upon the UV light irradiation for 1 min, the initial colorless solution turns red (Figure 1b), and a new absorption band appears at around 530 nm due to the closed ring form of DAE molecules with an increased π-conjugation length (Figure 1c).[48] The red color completely disappears after the visible light (λ > 400 nm) irradiation for 1 min, and the spectrum returns to the initial state, indicating the reversibility of photoswitchable molecular configurations.

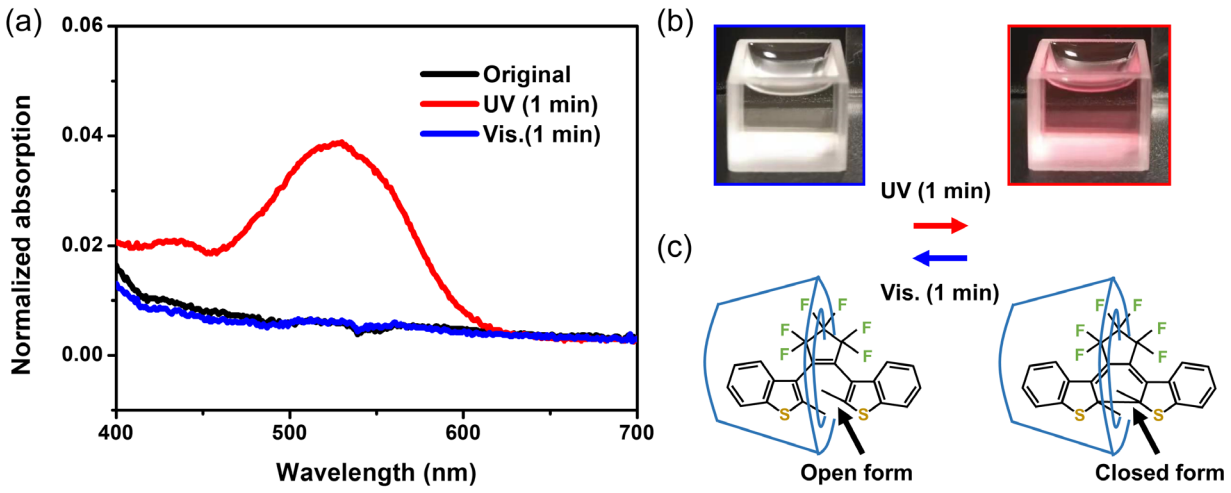

Figure 1. (a) Absorption spectra for the host (thiol-β-CD)-guest (DAE) molecular complex in DMF solution upon irradiation with UV (peak wavelength: 365 nm) and visible (λ > 400 nm) light. (b) Reversible color tuning of the host-guest complex in DMF solution after UV and visible light

irradiation. (c) Schematics of the open and closed molecular configurations of DAE encapsulated in thiol-β-CD under photoirradiation. Exposure to UV light switches the molecular complex into a photoactive ("on") state; re-illuminating the systems with visible light recovers to its "off" state.

Next, to demonstrate the light-controlled tuning ability of the photoactive molecule-complex-sandwiched MPoFNs comprised of Au NSs separated from an Au thin film by a SAM of host (thiol-β-CD)-guest (DAE) molecular complex as shown in Figure 2a and 2b, SERS spectroscopy is employed to confirm the switching between different Raman vibrational modes of the molecular complex under optical stimulus (alternating UV/visible light irradiation). Figure 2c shows the single-particle SERS spectra collected from an individual MPoFN under a UV-visible light illumination cycle. The original SERS spectra (black line) exhibit several Raman bands between 1200 and 1800 cm^{-1} that can be assigned to DAE with different forms. Among them four distinct Raman bands that centered at 1288, 1371, 1493 and 1587 cm^{-1} have shown reversible tuning after a UV-visible light exposure cycle. Concretely speaking, two intense bands (centered at 1288 and 1493 cm^{-1}) occurred in the spectrum after UV light illumination (red line) are not seen in other two spectra when the guest molecule is in the open form state. While for Raman bands peaked at 1371 and 1587 cm^{-1}, they only appear in the spectrum under original state and after visible light exposure (blue line). To verify whether all these Raman bands are from DAE in the molecular complex, we also measured Raman spectra of solids of guest (DAE) and host (thiol-β-CD) molecules, respectively (as seen in Figure S2a and S2b), and the result shows great consistency. Note that in Figure S2b, Raman peak at 2575 cm^{-1} occurs as the evidence of thiol groups bonded in β-CD.[49] Moreover, Raman peaks observed in the SERS spectrum can be considered as different vibrational modes. For example, in the open form of DAE molecules, Raman band at 1587 cm^{-1} corresponds to the stretching of C=C double bond in the hexafluoro cyclopentene. The band at 1288 cm^{-1} for

DAE molecule in the closed form state is attributed to the combination of four coupling modes: cyclopentene breathing mode, in-plane C=C-C bending of the central phenyl group, in-plane C=C-S bending of the thiophene and rocking mode of the methyl group. Note that the relative intensity of these vibrational modes in the SERS spectrum acquired with a polarized excitation strongly depends on the symmetry of the modes and the conformation of molecules sitting on the surface or the particle-film gap region.[50] For the molecular complex employed in our system, the transition moment of DAE in the CD cavity would change by photoirradiation, which is highly related to its structural symmetry.[46] Hence, the distinct Raman bands of DAE with different forms could reflect the molecular structural changes during the photoswitchable reaction.

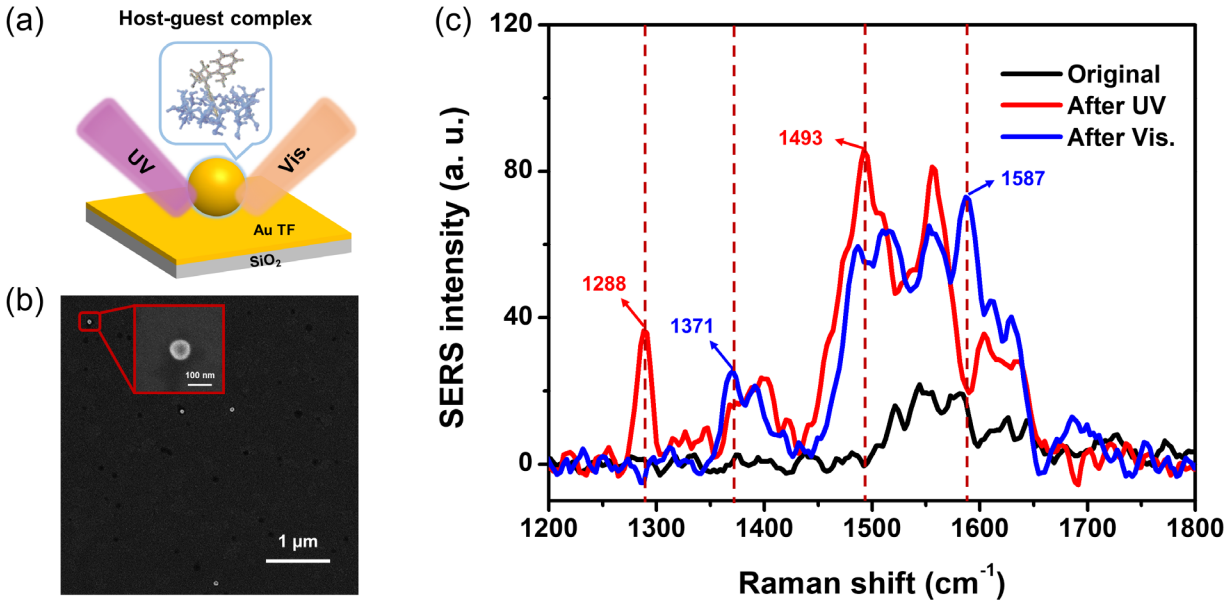

Figure 2. (a) Schematic representation of a photoactive host (thiol-β-CD)-guest (DAE) molecular complex-sandwiched MPoFN under UV/visible light irradiation. (b) High-resolution SEM image of individual active plasmonic molecular nanocavities. Inset demonstrates the enlarged view of a photoactive molecule-sandwiched MPoFN (marked by the red square). (c) SERS spectra (633 nm continuous wave (CW) laser excitation) of the selected photoswitchable molecule-sandwiched

MPoFN after UV and visible light illumination (acquisition time of 20 s for a laser power of about 0.01 mW).

When the molecular configurations of DAE switch under alternating irradiation with UV and visible light, the corresponding photo-induced refractive index change and conductance switching in the molecular junction could result in active modulation of plasmon resonance in the photoactive plasmonic molecular nanocavity. Inspired by this concept, dark-field scattering spectroscopy was exploited to investigate photoswitching effect of molecular complex on the plasmon resonance. As depicted in Figure 3a, the gap mode of a representative nanocavity initially peaks at 718 nm. After UV and visible light exposure, there is no perceivable peak shift in the scattering spectrum of the photoswitchable molecule-sandwiched nanocavity. To investigate the light-triggered photochromic effect on linear optical responses quantitatively, dark-field scattering characterization was carried out on dozens of photoactive molecule-sandwiched MPoFNs. On the one hand, the measured results show that the statistical wavelengths of the predominated scattering resonance under original state, after UV and after visible light illumination are nearly the same (about 722 nm, as shown in Figure S4); On the other hand, it is seen that the statistical peak intensity of the gap mode (722 nm) in plasmonic molecular nanocavities after UV light illumination is about 8% lower than that under initial state, and after the visible light illumination it almost recovers to the original level (Figure 3b). The barely shifted scattering resonance in our system may result from two parts: One is the non-resonant coupling between the plasmon resonance and photochromic molecule;[51] the other is the lack of functional groups (such as thiol group) that could provide a steadily conductive path in gold-molecule-gold nanojunctions through forming strong chemical bond.[45, 52, 53] To further understand aforementioned phenomena, we performed full-wave electromagnetic simulations to calculate scattering spectra of the photoactive

molecule-sandwiched MPoFN (see Supporting Information for details). The molecular layer is modeled as a dielectric layer with thickness d and a complex refractive index $n + ik$. In the simulation, we set n = 1.63 for the host-guest complex with both open and closed forms of DAE molecules according to the reported value.[54] For the molecular complex with open form of DAE molecules we set k = 0 because the absorption spectra of the molecular solution under original state and after visible light illumination are quite low within the measured wavelength range (Figure 1a). For the molecular nanocavity with open form of DAE molecules, we find that the predominated resonance wavelength of the scattering spectrum matches well with the statistical result (around 722 nm) under the experimental measurement when d = 2 nm (determined by the molecular length of DAE) as shown by the olive line in Figure 3c. For the MPoFN with closed form of DAE molecules, the calculated scattering spectrum agrees with the experimental observation when k = 0.013 (pink line in Figure 3c) in terms of about 8% lower peak intensity compared with the peak intensity when k = 0 and no clear shift of resonance wavelength occurred. Such non-zero loss of the molecular complex with closed form of DAE molecules is consistent with the experimental observation regarding that the molecular complex with DAE molecules after UV light illumination have much higher absorption (red line in Figure 1a). After obtaining the far-field scattering spectrum, we further calculated the near-field distributions of the MPoFN at three picked wavelengths (633, 720 and 850 nm) as shown in Figure 3d. Note that the near-field distributions of the MPoFN with open (k = 0) and closed (k = 0.013) forms of DAE molecules share same patterns. The surface averaged near-field enhancement factors of the MPoFN with open and closed forms of DAE molecules are labeled below the distribution patterns as shown in the second row. Clearly, all the enhancement factors (at picked wavelengths) of the MPoFN with DAE molecules (closed form) are only slightly smaller than those of the MPoFN with open form of

DAE molecules. This is due to the fact that the loss (k = 0.013) of DAE molecules with closed form is not large enough to significantly change both the linear far- and near-field optical responses of the photoactive plasmonic molecular nanocavity.

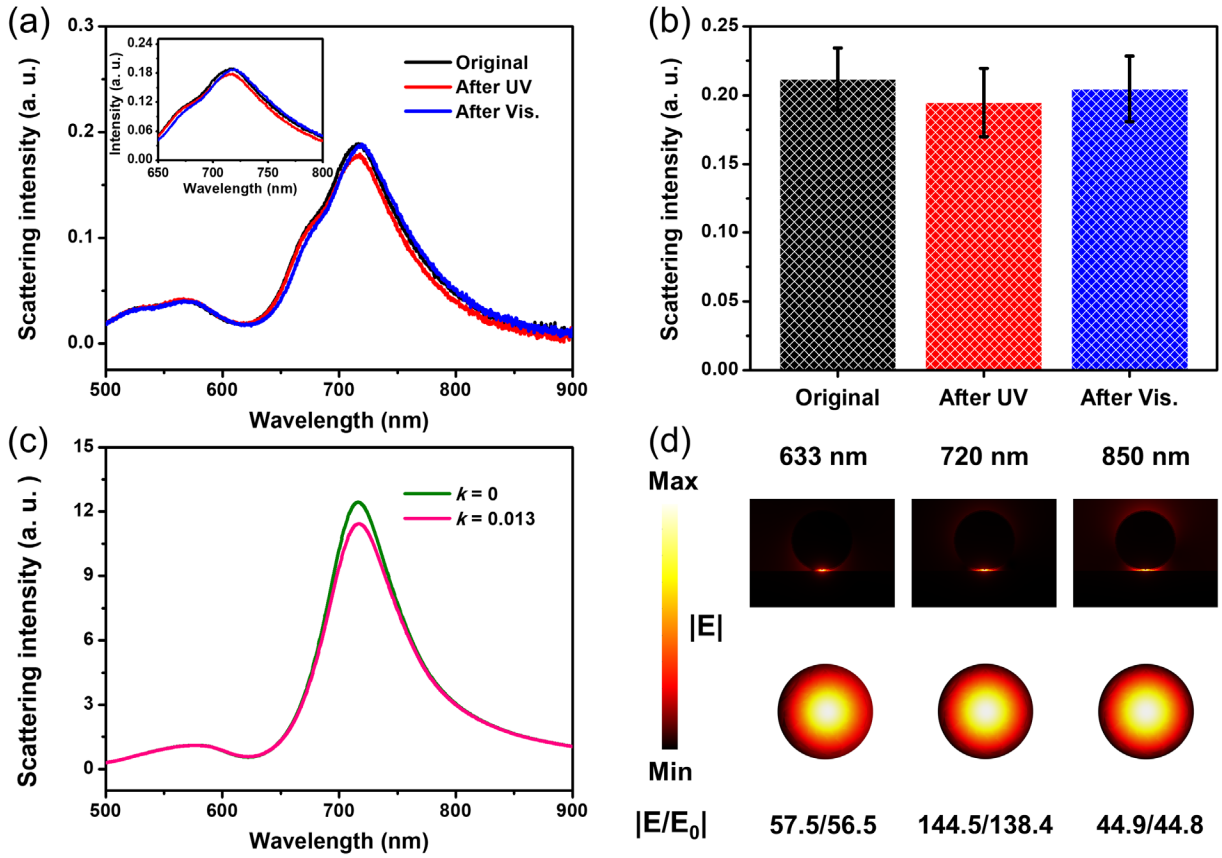

Figure 3. (a) Dark-field scattering spectra of the host-guest molecule-complex-sandwiched MPoFN taken during one UV-visible light exposure cycle. Reversible tuning of the coupled mode is shown in the inset. (b) Statistics of the measured peak intensities of the gap mode in the photoactive molecule-sandwiched MPoFN. The error bars represent standard deviations of the measured peak intensities for twenty plasmonic molecular nanocavities under different states. (c) Calculated scattering spectra of the MPoFN with open (k = 0) and closed (k = 0.013) forms of DAE molecules. (d) Distribution profiles of the electric field amplitude $|\mathbf{E}|$ at the vertical cut plane of the MPoFN (first row) and in the horizontal cut plane of the gap between the sphere and substrate (second row). Surface averaged (on the horizontal cut plane) near-field enhancement

factors $|\mathbf{E}/\mathbf{E_0}|$ of the MPoFN with open (closed) form of DAE molecules are labeled as former (latter) values below the distribution patterns as shown in the second row. $|\mathbf{E_0}|$ is the incident electric field amplitude.

To demonstrate all-optical control of nonlinear emissions, we carried out nonlinear optical spectroscopy on the photoactive plasmonic molecular nanocavity and chose SHG as the probe signal. It is well known that SH emission signals of metallic nanostructures highly depend on their localized near-field enhancements at fundamental excitation wavelengths: $I_{2\omega} \propto E_{\omega}^{4}$.[17, 55, 56] Particularly, the distribution of longitudinal vectorial light fields can be mapped using the nanoprobe (SHG from a metal nanocavity) as reported by our previous work.[18] Hence, the SHG intensity can be modulated through on- and off-plasmon resonance. However, in Figure 3a, no perceivable peak shift of the coupled mode was observed, which indicates that if we only consider the effect of plasmonic near-field enhancement on SHG signal, there will be a very limited space for nonlinear modulation in the plasmonic molecular nanocavity (also verified by numerical results in Figure 3d). Interestingly, a large modulation of the SHG emission was achieved in the photoactive molecular nanocavity during one UV-visible light illumination cycle (Figure 4a). More specifically, when we use 850 nm femtosecond (fs) laser (pulse width ~100 fs, repetition rate 80 MHz) as the excitation source, SHG intensity of the active plasmonic nanocavity exhibits a large increase after 15 min illumination of UV light (red dots and fitted curve in Figure 4a), then after illumination of visible light in the same amount of time, the intensity of SHG signal almost decreases to the original level (blue dots in Figure 4a). To better quantify the dynamic control of nonlinear response (SHG) in individual photoactive molecule-sandwiched MPoFNs, we integrated the area of SHG emission peaks and calculated the integral intensity of SHG signals in fourteen photochromic molecular nanocavities under different states. The results demonstrated that the

average integral intensities of SHG emissions after UV light irradiation are 2- to 3-fold larger than that under original state. After visible light illumination, SHG intensities decreased by 2 times compared to that after UV light irradiation, indicating the reversible tuning ability in the photochromic molecule-sandwiched MPoFN (see Figure 4b and Supporting Information for details). Note that the dwell time of pump laser at each pixel is extremely short (1.2 μs) during the scanning process to minimize fs laser-induced damage to the nanostructure. The average power and corresponding power density of fs laser are 0.3 mW and 3.16×10^4 W/cm^2, respectively (see Supporting Information for details). In addition, the dark-field scattering spectra of the molecular nanocavity collected before and after the SHG measurements indicate that there is a minute modification of particle-film gap morphology under multiple fs laser excitation (Figure S5),[57, 58] giving the perceivable difference between average integral SHG intensities under original state and after visible light irradiation (Figure 4b). In view of this consideration, we pay more attention to the variation trend of integral SHG intensities during a UV-visible light exposure cycle rather than the absolute SHG intensity value under a certain state. It is also worth noting that even under off-resonance excitation (850 nm), we can still optically modulate the emission intensity of SHG in this active molecular nanocavity. Therefore, the proposed active plasmonic molecular nanocavity can function as a versatile nonlinear plasmonics platform for all-optical control of optical harmonic generation at the nanoscale.

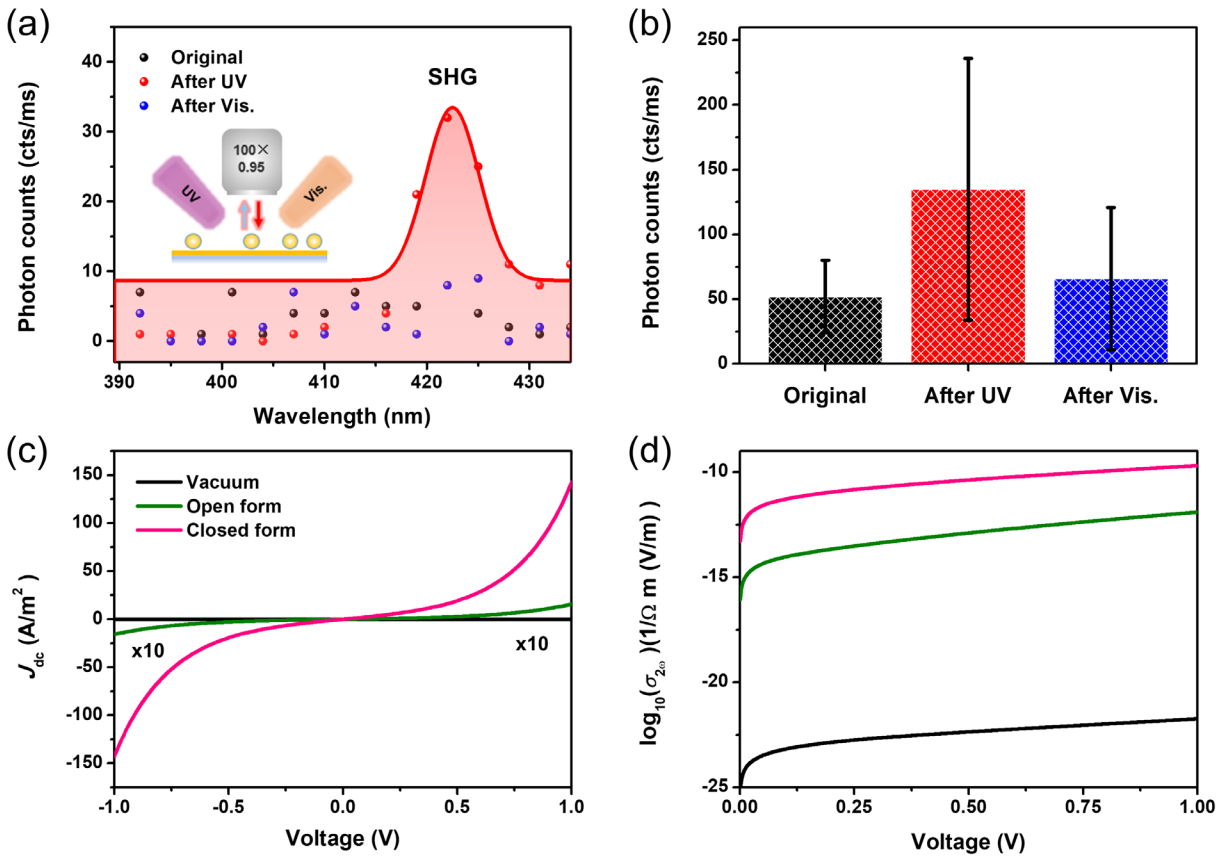

Figure 4. (a) Active tuning of SHG emissions in a photoactive plasmonic molecular nanocavity. The black, red and blue symbols represent measured SHG spectra of the nanocavity under original state, after UV and after visible light illumination, respectively. They are also denoted as the 1st, 2nd, 3rd SHG according to the measurement sequence. The solid line (red) is fitting to the SHG spectrum after UV light irradiation. Inset shows schematics of SHG excitation configuration under UV/visible light irradiation. (b) Statistics of the integral 1st, 2nd, 3rd SHG intensities in photoactive molecule-sandwiched MPoFNs. The error bars refer to standard deviations of the integral SHG intensities for fourteen plasmonic molecular nanocavities under different states. (c) Current density J_{dc} as a function of the dc bias V calculated by Simmons model with different barrier heights. (d) Logarithmic plot (base 10) of the calculated second-order nonlinear conductivity $\sigma_{2\omega}$ as a function of the asymmetric factor (virtual dc bias V) for different junctions (vacuum, DAE with open and closed forms).

To gain further insight into the physiochemical mechanism governing the observed SHG modulation, we calculated the near-field distributions of molecular nanocavities. From the results shown in Figure 3d, it is seen that at the nonlinear excitation wavelength (850 nm) the near-field enhancement factor of the junction with closed form of DAE molecules is slightly lower than that of the off-state junction. Therefore, the observed SHG modulation cannot be explained from the perspective of near-field enhancement. Instead, we employ the quantum conductivity theory (QCT) developed by Haus *et al.* to investigate the second-harmonic quantum conductivity (see Supporting Information for more details).[59, 60] Within the framework of photon-assisted tunneling (PAT) theory, the second-harmonic quantum conductivity ($\sigma_{2\omega}$) is given by[60]:

$$\sigma_{2\omega} = \left(\frac{ed}{2\hbar\omega}\right)^2 \left[J_{\mathrm{dc}}(eV) - \left(J_{\mathrm{dc}}(\hbar\omega + eV) + J_{\mathrm{dc}}(-\hbar\omega + eV)\right) + \frac{1}{2}\left(J_{\mathrm{dc}}(2\hbar\omega + eV) + J_{\mathrm{dc}}(-2\hbar\omega + eV)\right)\right] \quad (1)$$

where e is the electron charge, d is the barrier width (here and after we use 2 nm according to the numerical results shown in Figure 3c), $\hbar$ is the reduced Planck's constant, ω is the angular frequency of the excitation wave, m is the mass of electron, and J_{dc} is the current density of the junction under a dc bias. For simplicity, here we assume that charge transport in the MPoFN is in a direct tunneling manner, where junctions with different molecules can be regarded as Au-insulator-Au structures with different barrier heights (Figure S6). Based on the Simmons model, the direct tunneling current density J_{dc} of a metal-insulator-metal junction can be calculated as[61]:

$$J_{\mathrm{dc}} = J_0\left\{\varphi_{\mathrm{A}} \exp\left(-A\sqrt{\varphi_{\mathrm{A}}}\right) - (\varphi_{\mathrm{A}} + eV) \exp\left(-A\sqrt{\varphi_{\mathrm{A}} + eV}\right)\right\} \quad (2)$$

where φ_{A} is the average barrier height under a dc bias V, h is the Planck's constant, $J_0 = e/2\pi hs^2$, where s is the modified barrier width, and $A = 4\pi s\sqrt{2m}/h$. Figure 4c shows J_{dc} of junctions with

different forms of molecules (including vacuum junction) as a function of the applied dc bias V (see Supporting Information for details). Firstly, we see that the current densities of the junction with vacuum and open form of DAE molecules are much lower than that of the junction with closed form of DAE molecules by noticing that current densities of the former are amplified by 10 times for better visualization (black and olive curves). Secondly, we also note that J_{dc} is an odd function with respect to the applied dc bias V because both the material and the geometry are symmetrical in the configuration (Figure S6). On the basis of the second conclusion, we can expect that $\sigma_{2\omega}$ shall be zero when no dc bias is applied to the junction (i.e. $V = 0$). However, Huang *et al*. have shown that the *I-V* curve of the junction with DAE molecules is not exactly odd symmetric with respect to $V = 0$ due to the molecule-electrode interaction (see Supporting Information for details).[62] In addition, structural asymmetry in the MPoFN may further result in the difference of $|J_{\mathrm{dc}}|$ at the same V under positive and negative biases.[18] Considering above factors, we could calculate $\sigma_{2\omega}$ at the excitation frequency ω (λ = 850 nm in our experiment) by involving a virtual dc bias V in Equation (1) as an asymmetric factor to incorporate the asymmetry in real molecular junction though no actual dc bias is applied in our experiment. Figure 4d shows $\sigma_{2\omega}$ for different junctions as a function of the virtual dc bias V. Clearly, the value of $\sigma_{2\omega}$ for the nanojunction with closed form of DAE molecules is several orders of magnitude larger than that with vacuum and open form of DAE molecules as long as the virtual dc bias V is not zero. This implies that any broken of the odd symmetry of J_{dc} with respect to $V = 0$ will lead to dramatic differences of $\sigma_{2\omega}$ in junctions with vacuum, open and closed forms of DAE molecules. As a consequence, the experimentally observed SHG modulation can be qualitatively explained by the results shown in Figure 4d.

In conclusion, we have demonstrated dynamic control of optical responses in individual photoswitchable molecule-sandwiched MPoFNs under visible regime. To begin with, reversible tuning of the SERS and scattering resonance in the photoactive plasmonic molecular nanocavity was realized under a UV-visible light irradiation cycle. Note that the junction conductance can be controlled based on the light-switched photochromic effect while keeping the molecular length almost unchanged. Then the intensity of SHG signal was reversibly modulated under UV/visible light illumination and the mechanism behind this phenomenon was explained by quantum conductivity theory qualitatively. Overall, the study of this work is expected to open up new avenues for manipulating both linear and nonlinear plasmonic responses of metal-based nanophotonics devices with electrical, optical and chemical approaches commonly used in single-molecule-based nanoelectronics, thereby providing a plethora of opportunities for merging and reconciling nonlinear plasmonics and active plasmonics at the nanoscale.

ASSOCIATED CONTENT

Supporting Information.

The Supporting Information is available free of charge.

Experimental details of sample fabrication and additional optical spectroscopy of both host (guest) molecules and photoactive molecule-sandwiched MPoFNs, description of the numerical simulation.

AUTHOR INFORMATION

Corresponding Author

*Dangyuan Lei – Department of Materials Science and Engineering, City University of Hong Kong, 83 Tat Chee Avenue, Kowloon, Hong Kong S.A.R.; Email: dangylei@cityu.edu.hk

Authors

Danjun Liu – Department of Materials Science and Engineering, City University of Hong Kong, 83 Tat Chee Avenue, Kowloon, Hong Kong S.A.R.; Department of Applied Physics, The Hong Kong Polytechnic University, 11 Yuk Choi Road, Hung Hom, Hong Kong S.A.R; orcid.org/0000-0001-6842-5599

Yunxia Wang – Department of Materials Science and Engineering, City University of Hong Kong, 83 Tat Chee Avenue, Kowloon, Hong Kong S.A.R.

Qiang Zhang – College of Optoelectronics, and Key Lab of Advanced Transducers and Intelligent Control System of Ministry of Education, Taiyuan University of Technology, Taiyuan 030024, China

Ye Ming Qing – Department of Materials Science and Engineering, City University of Hong Kong, 83 Tat Chee Avenue, Kowloon, Hong Kong S.A.R.

Yaorong Wang – Department of Materials Science and Engineering, City University of Hong Kong, 83 Tat Chee Avenue, Kowloon, Hong Kong S.A.R.

Haitao Huang – Department of Applied Physics, The Hong Kong Polytechnic University, 11 Yuk Choi Road, Hung Hom, Hong Kong S.A.R.

Chi Wah Leung – Department of Applied Physics, The Hong Kong Polytechnic University, 11 Yuk Choi Road, Hung Hom, Hong Kong S.A.R.

Author Contributions

[#]D.J.L., Y.X.W. and Q.Z. contributed equally. The manuscript was written through contributions of all authors. All authors have given approval to the final version of the manuscript.

Funding Sources

We acknowledge the Research Grants Council of Hong Kong through the General Research Fund grant (15303417) and the ANR/RGC Joint Research Scheme grant (A-CityU101/20), and the National Natural Science Foundation of China (Grant No. 12004273).

Notes

The authors declare no competing financial interest.

ACKNOWLEDGMENT

D.J.L. appreciates the help of and valuable discussions with Dr. Siqi Li and Dr. Guangcan Li.

REFERENCES

(1) Li, J. F.; Huang, Y. F.; Ding, Y.; Yang, Z. L.; Li, S. B.; Zhou, X. S.; Fan, F. R.; Zhang, W.; Zhou, Z. Y.; Wu, D. Y.; Ren, B.; Wang, Z. L.; Tian, Z. Q. Shell-Isolated Nanoparticle-Enhanced Raman Spectroscopy. *Nature* **2010**, *464* (7287), 392-395.
(2) Langer, J.; Jimenez de Aberasturi, D.; Aizpurua, J.; Alvarez-Puebla, R. A.; Auguié, B.; Baumberg, J. J.; Bazan, G. C.; Bell, S. E. J.; Boisen, A.; Brolo, A. G.; Choo, J.; Cialla-May, D.; Deckert, V.; Fabris, L.; Faulds, K.; García de Abajo, F. J.; Goodacre, R.; Graham, D.; Haes, A. J.; Haynes, C. L.; Huck, C.; Itoh, T.; Käll, M.; Kneipp, J.; Kotov, N. A.; Kuang, H.; Le Ru, E. C.; Lee, H. K.; Li, J.-F.; Ling, X. Y.; Maier, S. A.; Mayerhöfer, T.; Moskovits, M.; Murakoshi, K.; Nam, J.-M.; Nie, S.; Ozaki, Y.; Pastoriza-Santos, I.; Perez-Juste, J.; Popp, J.; Pucci, A.; Reich, S.; Ren, B.; Schatz, G. C.; Shegai, T.; Schlücker, S.; Tay, L.-L.; Thomas, K. G.; Tian, Z.-Q.; Van Duyne, R. P.; Vo-Dinh, T.; Wang, Y.; Willets, K. A.; Xu, C.; Xu, H.; Xu, Y.; Yamamoto, Y. S.; Zhao, B.; Liz-Marzán, L. M. Present and Future of Surface-Enhanced Raman Scattering. *ACS Nano* **2020**, *14* (1), 28-117.
(3) Li, J.-F.; Li, C.-Y.; Aroca, R. F. Plasmon-Enhanced Fluorescence Spectroscopy. *Chem. Soc. Rev.* **2017**, *46* (13), 3962-3979.
(4) Roelli, P.; Galland, C.; Piro, N.; Kippenberg, T. J. Molecular Cavity Optomechanics as a Theory of Plasmon-Enhanced Raman Scattering. *Nat. Nanotechnol.* **2016**, *11* (2), 164-169.
(5) Van Nieuwstadt, J. A. H.; Sandtke, M.; Harmsen, R. H.; Segerink, F. B.; Prangsma, J. C.; Enoch, S.; Kuipers, L. Strong Modification of the Nonlinear Optical Response of Metallic Subwavelength Hole Arrays. *Phys. Rev. Lett.* **2006**, *97* (14), 146102.
(6) Liu, S.-D.; Leong, E. S. P.; Li, G.-C.; Hou, Y.; Deng, J.; Teng, J. H.; Ong, H. C.; Lei, D. Y. Polarization-Independent Multiple Fano Resonances in Plasmonic Nonamers for Multimode-Matching Enhanced Multiband Second-Harmonic Generation. *ACS Nano* **2016**, *10* (1), 1442-1453.

(7) Lassiter, J. B.; Chen, X.; Liu, X.; Ciracì, C.; Hoang, T. B.; Larouche, S.; Oh, S.-H.; Mikkelsen, M. H.; Smith, D. R. Third-Harmonic Generation Enhancement by Film-Coupled Plasmonic Stripe Resonators. *ACS Photonics* **2014**, *1* (11), 1212-1217.
(8) Hanke, T.; Krauss, G.; Träutlein, D.; Wild, B.; Bratschitsch, R.; Leitenstorfer, A. Efficient Nonlinear Light Emission of Single Gold Optical Antennas Driven by Few-Cycle Near-Infrared Pulses. *Phys. Rev. Lett.* **2009**, *103* (25), 257404.
(9) Wang, B.-L.; Ren, M.-L.; Li, J.-F.; Li, Z.-Y. Plasmonic Coupling Effect between Two Gold Nanospheres for Efficient Second-Harmonic Generation. *J. Appl. Phys.* **2012**, *112* (8), 083102.
(10) Danckwerts, M.; Novotny, L. Optical Frequency Mixing at Coupled Gold Nanoparticles. *Phys. Rev. Lett.* **2007**, *98* (2), 026104.
(11) Zhang, Q.; Liu, D.; Ren, Q.; Panoiu, N. C.; Lin, L.; Ye, J.; Huang, Y.; Liu, S.-D.; Leung, C. W.; Lei, D. Probing Electron Transport in Plasmonic Molecular Junctions with Two-Photon Luminescence Spectroscopy. *Nanophotonics* **2021**, *10* (9), 2467-2479.
(12) Schuck, P. J.; Fromm, D. P.; Sundaramurthy, A.; Kino, G. S.; Moerner, W. E. Improving the Mismatch between Light and Nanoscale Objects with Gold Bowtie Nanoantennas. *Phys. Rev. Lett.* **2005**, *94* (1), 017402.
(13) Han, F.; Guan, Z.; Tan, T. S.; Xu, Q.-H. Size-Dependent Two-Photon Excitation Photoluminescence Enhancement in Coupled Noble-Metal Nanoparticles. *ACS Appl. Mater. Interfaces* **2012**, *4* (9), 4746-4751.
(14) Ueno, K.; Juodkazis, S.; Mizeikis, V.; Sasaki, K.; Misawa, H. Clusters of Closely Spaced Gold Nanoparticles as a Source of Two-Photon Photoluminescence at Visible Wavelengths. *Adv. Mater.* **2008**, *20* (1), 26-30.
(15) Dadap, J. I.; Shan, J.; Eisenthal, K. B.; Heinz, T. F. Second-Harmonic Rayleigh Scattering from a Sphere of Centrosymmetric Material. *Phys. Rev. Lett.* **1999**, *83* (20), 4045.
(16) Wang, F. X.; Rodríguez, F. J.; Albers, W. M.; Ahorinta, R.; Sipe, J. E.; Kauranen, M. Surface and Bulk Contributions to the Second-Order Nonlinear Optical Response of a Gold Film. *Phys. Rev. B* **2009**, *80* (23), 233402.
(17) Shen, S.; Meng, L.; Zhang, Y.; Han, J.; Ma, Z.; Hu, S.; He, Y.; Li, J.; Ren, B.; Shih, T.-M.; Wang, Z.; Yang, Z.; Tian, Z. Plasmon-Enhanced Second-Harmonic Generation Nanorulers with Ultrahigh Sensitivities. *Nano Lett.* **2015**, *15* (10), 6716-6721.
(18) Li, G.-C.; Lei, D.; Qiu, M.; Jin, W.; Lan, S.; Zayats, A. V. Light-Induced Symmetry Breaking for Enhancing Second-Harmonic Generation from an Ultrathin Plasmonic Nanocavity. *Nat. Commun.* **2021**, *12* (1), 4326.
(19) Hajisalem, G.; Nezami, M. S.; Gordon, R. Probing the Quantum Tunneling Limit of Plasmonic Enhancement by Third Harmonic Generation. *Nano Lett.* **2014**, *14* (11), 6651-6654.
(20) Grady, N. K.; Knight, M. W.; Bardhan, R.; Halas, N. J. Optically-Driven Collapse of a Plasmonic Nanogap Self-Monitored by Optical Frequency Mixing. *Nano Lett.* **2010**, *10* (4), 1522-1528.
(21) Hajisalem, G.; Ahmed, A.; Pang, Y.; Gordon, R. Plasmon Hybridization for Enhanced Nonlinear Optical Response. *Opt. Express* **2012**, *20* (28), 29923-29930.
(22) Lévêque, G.; Martin, O. J. F. Optical Interactions in a Plasmonic Particle Coupled to a Metallic Film. *Opt. Express* **2006**, *14* (21), 9971-9981.
(23) Mock, J. J.; Hill, R. T.; Degiron, A.; Zauscher, S.; Chilkoti, A.; Smith, D. R. Distance-Dependent Plasmon Resonant Coupling between a Gold Nanoparticle and Gold Film. *Nano Lett.* **2008**, *8* (8), 2245-2252.

(24) Kongsuwan, N.; Demetriadou, A.; Horton, M.; Chikkaraddy, R.; Baumberg, J. J.; Hess, O. Plasmonic Nanocavity Modes: From Near-Field to Far-Field Radiation. *ACS Photonics* **2020**, *7* (2), 463-471.
(25) Chikkaraddy, R.; Zheng, X.; Benz, F.; Brooks, L. J.; De Nijs, B.; Carnegie, C.; Kleemann, M.-E.; Mertens, J.; Bowman, R. W.; Vandenbosch, G. A. E.; Moshchalkov, V. V.; Baumberg, J. J. How Ultranarrow Gap Symmetries Control Plasmonic Nanocavity Modes: From Cubes to Spheres in the Nanoparticle-on-Mirror. *ACS Photonics* **2017**, *4* (3), 469-475.
(26) Sigle, D. O.; Kasera, S.; Herrmann, L. O.; Palma, A.; De Nijs, B.; Benz, F.; Mahajan, S.; Baumberg, J. J.; Scherman, O. A. Observing Single Molecules Complexing with Cucurbit [7] uril through Nanogap Surface-Enhanced Raman Spectroscopy. *J. Phys. Chem. Lett.* **2016**, *7* (4), 704-710.
(27) Mubeen, S.; Zhang, S.; Kim, N.; Lee, S.; Krämer, S.; Xu, H.; Moskovits, M. Plasmonic Properties of Gold Nanoparticles Separated from a Gold Mirror by an Ultrathin Oxide. *Nano Lett.* **2012**, *12* (4), 2088-2094.
(28) Liu, D.; Wu, T.; Zhang, Q.; Wang, X.; Guo, X.; Su, Y.; Zhu, Y.; Shao, M.; Chen, H.; Luo, Y.; Lei, D. Probing the in-Plane Near-Field Enhancement Limit in a Plasmonic Particle-on-Film Nanocavity with Surface-Enhanced Raman Spectroscopy of Graphene. *ACS Nano* **2019**, *13* (7), 7644-7654.
(29) Ciracì, C.; Hill, R. T.; Mock, J. J.; Urzhumov, Y.; Fernández-Domínguez, A. I.; Maier, S. A.; Pendry, J. B.; Chilkoti, A.; Smith, D. R. Probing the Ultimate Limits of Plasmonic Enhancement. *Science* **2012**, *337* (6098), 1072-1074.
(30) Zhu, W.; Esteban, R.; Borisov, A. G.; Baumberg, J. J.; Nordlander, P.; Lezec, H. J.; Aizpurua, J.; Crozier, K. B. Quantum Mechanical Effects in Plasmonic Structures with Subnanometre Gaps. *Nat. Commun.* **2016**, *7* (1), 1-14.
(31) Xu, D.; Xiong, X.; Wu, L.; Ren, X.-F.; Png, C. E.; Guo, G.-C.; Gong, Q.; Xiao, Y.-F. Quantum Plasmonics: New Opportunity in Fundamental and Applied Photonics. *Adv. Opt. Photonics* **2018**, *10* (4), 703-756.
(32) Kongsuwan, N.; Demetriadou, A.; Chikkaraddy, R.; Benz, F.; Turek, V. A.; Keyser, U. F.; Baumberg, J. J.; Hess, O. Suppressed Quenching and Strong-Coupling of Purcell-Enhanced Single-Molecule Emission in Plasmonic Nanocavities. *ACS Photonics* **2018**, *5* (1), 186-191.
(33) Chikkaraddy, R.; De Nijs, B.; Benz, F.; Barrow, S. J.; Scherman, O. A.; Rosta, E.; Demetriadou, A.; Fox, P.; Hess, O.; Baumberg, J. J. Single-Molecule Strong Coupling at Room Temperature in Plasmonic Nanocavities. *Nature* **2016**, *535* (7610), 127-130.
(34) Di Martino, G.; Turek, V. A.; Lombardi, A.; Szabó, I.; De Nijs, B.; Kuhn, A.; Rosta, E.; Baumberg, J. J. Tracking Nanoelectrochemistry Using Individual Plasmonic Nanocavities. *Nano Lett.* **2017**, *17* (8), 4840-4845.
(35) Di Martino, G.; Turek, V. A.; Tserkezis, C.; Lombardi, A.; Kuhn, A.; Baumberg, J. J. Plasmonic Response and SERS Modulation in Electrochemical Applied Potentials. *Faraday Discuss.* **2017**, *205*, 537-545.
(36) Cormier, S.; Ding, T.; Turek, V.; Baumberg, J. J. Actuating Single Nano-Oscillators with Light. *Adv. Optical Mater.* **2018**, *6* (6), 1701281.
(37) Zhang, C.; Li, D.; Zhang, G.; Wang, X.; Mao, L.; Gan, Q.; Ding, T.; Xu, H. Switching Plasmonic Nanogaps between Classical and Quantum Regimes with Supramolecular Interactions. *Sci. Adv.* **2022**, *8* (5), 1-6.

(38) Wurtz, G. A.; Pollard, R.; Hendren, W.; Wiederrecht, G. P.; Gosztola, D. J; Podolskiy, V. A.; Zayats, A. V. Designed Ultrafast Optical Nonlinearity in a Plasmonic Nanorod Metamaterial Enhanced by Nonlocality. *Nat. Nanotechnol.* **2011**, *6* (2), 107-111.
(39) MacDonald, K. F.; Sámson, Z. L.; Stockman, M. I.; Zheludev, N. I. Ultrafast Active Plasmonics. *Nat. Photonics* **2009**, *3* (1), 55-58.
(40) Nishi, H.; Asahi, T.; Kobatake, S. Light-Controllable Surface Plasmon Resonance Absorption of Gold Nanoparticles Covered with Photochromic Diarylethene Polymers. *J. Phys. Chem. C* **2009**, *113* (40), 17359-17366.
(41) Moilanen, A. J.; Hakala, T. K.; Törmä, P. Active Control of Surface Plasmon–Emitter Strong Coupling. *ACS Photonics* **2018**, *5* (1), 54-64.
(42) Dürr, H.; Bouas-Laurent, H. *Photochromism: Molecules and Systems*; Elsevier, **2003**.
(43) Irie, M.; Fukaminato, T.; Matsuda, K.; Kobatake, S. Photochromism of Diarylethene Molecules and Crystals: Memories, Switches, and Actuators. *Chem. Rev.* **2014**, *114* (24), 12174-12277.
(44) Irie, M.; Uchida, K. Synthesis and Properties of Photochromic Diarylethenes with Heterocyclic Aryl Groups. *Bull. Chem. Soc. Jpn.* **1998**, *71* (5), 985-996.
(45) Jia, C.; Migliore, A.; Xin, N.; Huang, S.; Wang, J.; Yang, Q.; Wang, S.; Chen, H.; Wang, D.; Feng, B.; Liu, Z.; Zhang, G.; Qu, D.-H.; Tian, H.; Ratner, M. A.; Xu, H. Q.; Nitzan, A.; Guo, X. Covalently Bonded Single-Molecule Junctions with Stable and Reversible Photoswitched Conductivity. *Science* **2016**, *352* (6292), 1443-1445.
(46) Takeshita, M.; Kato, N.; Kawauchi, S.; Imase, T.; Watanabe, J.; Irie, M. Photochromism of Dithienylethenes Included in Cyclodextrins. *J. Org. Chem.* **1998**, *63* (25), 9306-9313.
(47) Irie, M.; Miyatake, O.; Uchida, K. Blocked Photochromism of Diarylethenes. *J. Am. Chem. Soc.* **1992**, *114* (22), 8715-8716.
(48) Matsuda, K.; Yamaguchi, H.; Sakano, T.; Ikeda, M.; Tanifuji, N.; Irie, M. Conductance Photoswitching of Diarylethene–Gold Nanoparticle Network Induced by Photochromic Reaction. *J. Phys. Chem. C* **2008**, *112* (43), 17005-17010.
(49) Michota, A.; Bukowska, J. Surface-Enhanced Raman Scattering (SERS) of 4-Mercaptobenzoic Acid on Silver and Gold Substrates. *J. Raman Spectrosc*. **2003**, *34* (1), 21-25.
(50) Julien-Rabant, C.; Débarre, A.; Métivier, R.; Laurent, G. Single Particle SERS Signal on Gold Nanorods: Comparative Study of Diarylethene Photochromic Isomers. *J. Opt.* **2015**, *17* (11), 114018.
(51) Wilson, W. M.; Stewart, J. W.; Mikkelsen, M. H. Surpassing Single Line Width Active Tuning with Photochromic Molecules Coupled to Plasmonic Nanoantennas. *Nano Lett.* **2018**, *18* (2), 853-858.
(52) Cui, X.; Qin, F.; Lai, Y.; Wang, H.; Shao, L.; Chen, H.; Wang, J.; Lin, H.-q. Molecular Tunnel Junction-Controlled High-Order Charge Transfer Plasmon and Fano Resonances. *ACS Nano* **2018**, *12* (12), 12541-12550.
(53) Benz, F.; Tserkezis, C.; Herrmann, L. O.; De Nijs, B.; Sanders, A.; Sigle, D. O.; Pukenas, L.; Evans, S. D.; Aizpurua, J.; Baumberg, J. J. Nanooptics of Molecular-Shunted Plasmonic Nanojunctions. *Nano Lett.* **2015**, *15* (1), 669-674.
(54) Vazquez, A. J.; Nudelman, N. S. Ring Opening/Closure Reactions of Novel Diheteroarylethenes Derivatives. Solvent Effects. *J. Phys. Org. Chem.* **2012**, *25* (11), 925-932.
(55) Butet, J.; Brevet, P.-F.; Martin, O. J. F. Optical Second Harmonic Generation in Plasmonic Nanostructures: From Fundamental Principles to Advanced Applications. *ACS Nano* **2015**, *9* (11), 10545-10562.

(56) Davidson, R. B.; Yanchenko, A.; Ziegler, J. I.; Avanesyan, S. M.; Lawrie, B. J.; Haglund, Jr, R. F. Ultrafast Plasmonic Control of Second Harmonic Generation. *ACS Photonics* **2016**, *3* (8), 1477-1481.
(57) Tserkezis, C.; Esteban, R.; Sigle, D. O.; Mertens, J.; Herrmann, L. O.; Baumberg, J. J.; Aizpurua, J. Hybridization of Plasmonic Antenna and Cavity Modes: Extreme Optics of Nanoparticle-on-Mirror Nanogaps. *Phys. Rev. A* **2015**, *92* (5), 053811.
(58) Elliott, E.; Bedingfield, K.; Huang, J.; Hu, S.; De Nijs, B.; Demetriadou, A.; Baumberg, J. J. Fingerprinting the Hidden Facets of Plasmonic Nanocavities. *ACS Photonics* **2022**, *9* (8), 2643-2651.
(59) Haus, J. W.; De Ceglia, D.; Vincenti, M. A.; Scalora, M. Nonlinear Quantum Tunneling Effects in Nanoplasmonic Environments: Two-Photon Absorption and Harmonic Generation. *J. Opt. Soc. Am. B* **2014**, *31* (6), A13-A19.
(60) Haus, J. W.; De Ceglia, D.; Vincenti, M. A.; Scalora, M. Quantum Conductivity for Metal–Insulator–Metal Nanostructures. *J. Opt. Soc. Am. B* **2014**, *31* (2), 259-269.
(61) Simmons, J. G. Generalized Formula for the Electric Tunnel Effect between Similar Electrodes Separated by a Thin Insulating Film. *J. Appl. Phys.* **1963**, *34* (6), 1793-1803.
(62) Huang, J.; Li, Q.; Ren, H.; Su, H.; Shi, Q. W.; Yang, J. Switching Mechanism of Photochromic Diarylethene Derivatives Molecular Junctions. *J. Chem. Phys.* **2007**, *127* (9), 094705.

For Table of Contents Only